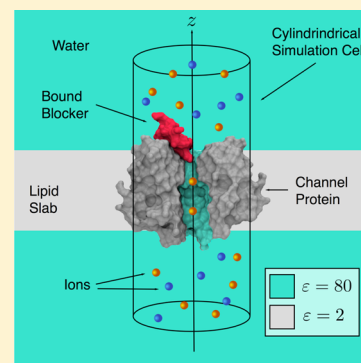


Extension of Brownian Dynamics for Studying Blockers of Ion Channels

Dan Gordon* and Shin-Ho Chung

Research School of Biology, Building 46, The Australian National University, Canberra, ACT 0200 Australia

ABSTRACT: We present new Brownian dynamics techniques for studying blockers of ion channels. By treating the channel as a fixed body, simulating the blocker molecules using rigid bodies, and using an implicit water force field with explicit ions, we are able to carry out fast simulations that can be used to investigate the dynamics of block and unblock, deduce binding modes, and calculate binding affinities. We test our program using the NavAb bacterial sodium channel, whose structure was recently solved (Payandeh et al. *Nature*, 2011, 475, 353–358) in conjunction with the μ -conotoxin PIIIA blocker. We derive an ohmic current–voltage relationship for channel permeation, calculate potentials of mean force for blocker unbinding, and deduce multiple binding modes for the blocker. Our results are shown to be compatible with other computational and experimental results. Finally, we discuss future improvements such as the inclusion of flexible side chains. After these improvements are carried out, we anticipate our program will be an extremely useful new tool that could be used to help develop new drugs to treat a range of ion-channel related diseases.



INTRODUCTION

Research into ion channel blocker molecules is of great clinical importance, as the ability to selectively block various types of ion channel would allow new treatments to be developed for a range of cardiac, neurological, and autoimmune conditions.^{1–3} There are various means by which ion channel blockers can operate, including internal and external block by small drug-like molecules⁴ or external block by larger toxin molecules occurring in the venoms of many creatures.^{3–6} In each of these cases, computationally modeling the interactions between these blocker molecules and ion channels is expected to greatly help in the design of new drugs that will treat channelopathies. Unfortunately, such modeling has also proved to be extremely challenging. Molecular docking, molecular dynamics, regression modeling (QSAR), and Brownian dynamics have all been used to model ion channel blockers, with each having advantages and disadvantages, but none really providing the combination of speed and accuracy that is ultimately needed. Thus, research into computational methods for investigating how blockers, including large polypeptide toxins, interact with ion channels represents an ongoing and pressing need.

In this paper, we present new Brownian dynamics methods for modeling channel-blocker systems. The use of Brownian dynamics to study ion channel blockers has several advantages. First, long time scale simulations can be performed, without the need to use extremely costly purpose built hardware.⁷ Simulations can investigate the interaction between channel blockers and permeant ions and be used to answer questions about the effectiveness of block, leaky block, or binding and unbinding mechanics, for example. Second, the simulations can be used to derive potentials of mean force, free energies of binding, and binding affinities. Similar calculations have been performed using molecular dynamics,^{8–15} but they are computationally expensive,

and for practical simulation times, the results are somewhat open to question. Brownian dynamics simulations are able to reach much longer time scales and can therefore provide a more complete exploration of possible binding configurations. Third, it is possible to use Brownian dynamics as a docking protocol;¹⁶ this has the advantage of implicitly taking into account entropic contributions to the free energy that are associated with the rotational and translational motion of the blocker and, in the case of ion channels, is also able to take into account the effect of bound ions in channel pores. Fourth, implicit solvent electrostatics can be to some extent more reliable than molecular dynamics simulations due to the slow relaxation of water in the latter; this is part of the reason for the relative success of the MM-PBSA method,^{17,18} for example. Lastly, the ability to perform rapid and computationally efficient simulations makes Brownian dynamics a good testing ground for the development of new techniques such as free energy methods.

In the past, Brownian dynamics simulations have proved to be of great help in elucidating the mechanisms of ion permeation across biological ion channels.¹⁹ To build on this success, we have implemented several new developments in our program. We use rigid-body simulations,¹³ extend the electrostatics methods used in previous Brownian dynamics simulations,^{13,19,20} and add a simple term to our force field that represents hydrophobic and other nonpolar interactions. We employ direct integration and umbrella sampling techniques to calculate the potentials of mean force for ions and blockers in the presence of the channel.

To test our new techniques, we apply them to the NavAb sodium channel, for which a crystal structure has been recently published²¹

Received: October 2, 2012

Revised: November 12, 2012

Published: November 16, 2012

along with the μ -conotoxin PIIIA blocker.^{14,22–25} We first test the ability of the force field to model the permeation characteristics of the channel and show that the results are in reasonable agreement with experimental^{26,27} and computational^{28,29} studies. This provides validation for the channel energetics of our model. We next look at the spontaneous binding of the blocker to the channel during simulations. The binding is shown to occur on easily reachable time scales and to be of some help in the determination of binding modes. Finally, we derive potentials of mean force (PMFs) for blocker unbinding which agree reasonably well with experimental binding energies^{30,31} and molecular dynamics calculations¹⁴ for two binding modes of the blocker. Thus, in the case of this particular channel and blocker, our model is shown to be consistent with a number of computational and experimental results.

We conclude with a discussion of future prospects for improving our simulation. The computational study of molecules binding to ion-channels faces two distinct challenges, in the case where slow, fully atomistic simulations are not employed. First is the need for flexibility, so that molecules are able to spatially conform closely to each other. We aim to implement flexible side chains in the near future. Second is the need for a fast and accurate implicit solvent force field. In this initial study, we use an approximate parameter set to produce sensible behavior on one particular channel-blocker system. In the future, it will be desirable to devise a broader and more systematic parametrization of the force field, based on rigorous physical principles. Nonetheless, we believe that the ability to realistically model the channel-blocker dynamics represents a significant advancement in the field.

THEORY AND METHODS

Simulation Cell. Our Brownian dynamics simulation cell, Figure 1, is a cylinder with an approximate length of 100 Å and

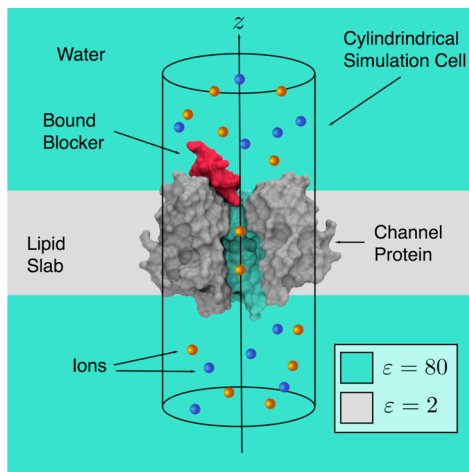


Figure 1. Brownian dynamics simulation cell. Aqueous regions of high dielectric constant are shown in aqua, and low dielectric constant regions in gray. The rigid blocker is shown in red, and ions are depicted as blue and orange spheres. The cylinder represents a physical barrier to ions and blocker molecules.

radius 30 Å. The axis of the cylinder runs along the z axis and coincides with the central axis of the channel pore. The dimensions of the cell are much larger than the Debye length, which is around 8 Å for a concentration of 140 mM. Therefore, the pore region should be well shielded from any modest

artifacts due to the hard cylindrical cell boundary. The channel itself consists of a rigid atomic model, positioned with the pore axis running down the central (z) axis of the channel, and roughly centered about $z = 0$. Thus the simulation cell contains intracellular and extracellular reservoirs separated by the channel protein. The charges and masses of all hydrogen atoms in the channel (and also the blocker) are combined with their parent atoms. The channel is also embedded in a membrane slab, also impermeable to ions, that runs across the simulation cell.

The correct ion concentration is maintained in the system using the grand canonical Monte Carlo technique.^{32,33} Absorbing boundaries, consisting of 10 Å thick disc shaped regions, are located at the top and bottom of the cylindrical cell. Ions may be created and destroyed in these regions, with probabilities that give rise to a grand canonical ensemble that maintains correct ion concentrations in the system.

Equations of Motion and Motion Algorithms. The simulation includes two types of mobile objects: monatomic ions and rigid-body blocker molecules. The ions are simulated using the Langevin equation

$$\begin{aligned} d\mathbf{r}_i(t) &= \mathbf{v}_i(t)dt \\ d\mathbf{v}_i(t) &= \frac{1}{m_i} \mathbf{f}_{s,i}(\{\mathbf{r}(t)\})dt - \gamma_i \mathbf{v}_i(t)dt - \frac{1}{m_i} R_i d\mathbf{w}_i \end{aligned} \quad (1)$$

where \mathbf{r}_i and \mathbf{v}_i are the position and velocity of the i th ion, m is its mass, $\mathbf{f}_{s,i}$ is the position dependent systematic force, γ_i is the friction coefficient, R_i is the strength of the random force, and $d\mathbf{w}_i$ is a Wiener process (Brownian motion). R is related to γ through the fluctuation–dissipation theorem:³⁴ $R_i^2 = 2m_i\gamma_i kT$. This equation of motion is solved using the algorithm of van Gunsteren and Berendsen.^{19,35}

Each blocker molecule is treated as a rigid body whose position and orientation in space can be described by six parameters: three Cartesian coordinates for the center of mass and three Euler angles for the rotational orientation around the center of mass. Unlike the ions, which live in a Cartesian space, the noncommutative rotational algebra complicates the equations of motion. In addition, the friction is no longer described by a single number, γ , but rather by a 6×6 friction tensor, meaning the frictional force varies depending on the orientation of the molecule relative to its velocity, and may act in a different direction from the velocity. We can represent the position and orientation of the blocker by a seven component object X . The first three components of X are the Cartesian center of mass coordinates, in the body frame as opposed to the laboratory frame, and the next four describe a quaternion specifying the orientation. Normalization of the quaternion removes one degree of freedom meaning that X lives in a six-dimensional manifold. The velocity and angular velocity are likewise represented by a six component object V . The equations of motion can then be written as a tensor equation:

$$\begin{aligned} dX_i &= (c_{ijk}X_jV_k + d_{ijk}X_jX_kV_l)dt \\ dV_i &= (a_i(X) + b_{ijk}V_jV_k - \gamma_{ij}V_j)dt + s_{ij}d\mathbf{w}_j \end{aligned} \quad (2)$$

Here, b , c , d , γ , and s are tensors. The term proportional to c is just the usual $x = vt$ relation but includes a transformation between the body and lab frame. a is the acceleration and angular acceleration due to the force and torque on the body. The term proportional to γ is a frictional term, analogous to eq 1 except that γ is now a tensor. Similarly, the term proportional to s is analogous to the

random force term in eq 1, except that s is a tensor. The terms proportional to d and b do not have analogs in the standard Langevin equation; they describe purely rotational effects. From an algorithmic perspective, there are two problems. First, the tensor nature of the equation complicates the development of sophisticated specialized algorithms such as that which van-Gunsteren and Berendsen algorithm used for the ions. Second, the quadratic velocity dependence in the second equation for V precludes standard solution methods. The equations of motion are instead solved using our own algorithm.³⁶ The friction tensor is derived using the HYDROPRO program,³⁷ based hydrodynamic calculations.

Force Field. Developing a good implicit water force field is difficult. In the current study, we use several approximations, with parameters being adjusted to give realistic potentials of mean force, ionic permeation results, and blocker binding. This has resulted in a force field that is qualitatively correct but which may require a more rigorous tuning procedure to accurately model a range of channels and blockers. The force field can be divided into terms representing steric atom–atom forces, channel and solvent mediated electrostatic forces involving single ions or pairs of ions, nonpolar hydration forces, and additional forces to account for the formation of salt-bridges and hydrogen bonds.

Steric Forces. Steric atom–atom forces prevent atoms from overlapping. The repulsive part of the Lennard-Jones potential is used, following the Weeks–Chandler–Andersen (WCA) decomposition.³⁸ Close contact forces can vary greatly with atomic radius, and a realistic treatment of such forces is intimately tied up with the other details of the force field such as the approximations used in deriving the electrostatics and the treatment of solvation, making the optimum choice of radii highly model dependent. In the original WCA model, the location of the minimum of the Lennard-Jones potential was used to define the point at which the WCA potential goes to zero, but this choice may not be ideal.³⁹ In this study, we uniformly scale the atomic radii by a factor of 0.85 for the purpose of calculating steric atom–atom interactions. This choice seems to allow the blocker to correctly dock in the pore, whereas using the unscaled Lennard-Jones radii clearly leads to clashes that prevent the correct behavior.

Steric/short-range interactions involving two ions are handled in a more sophisticated manner than other atom–atom short-range forces, using a solvent mediated short-range potential fitted to molecular dynamics simulations.⁴⁰ This kind of fitting is not practical for nonion atoms, because of the large number of atom types that would need to be taken into account and because the forces would depend on the arrangement of other protein atoms that surround the two atoms in question. The fitted potential is able to encapsulate steric forces, hydration effects, and the dispersive van der Waals forces due to the ions themselves as well as the surrounding water.

Electrostatic Forces. Electrostatic channel and solvent mediated forces are generated by the static partial charges in the channel, plus the mobile charges, in the presence of the dielectric boundary of the channel and lipid system (see Figure 1). These forces can be divided into two categories.

In the first category are forces that are due to the electric field originating from the fixed charges in the channel, and also from the membrane potential, in the absence of all other changes. Since the channel is fixed, its electric field can be calculated in a single calculation and then stored in a three-dimensional lookup table, which is interpolated during the simulation. To generate this lookup table, a dielectric map is first defined from within the APBS program⁴¹ based on the molecular surface. Atomic radii

suitable for solving Poisson's equation are used, taken from Nina et al.⁴² A high dielectric constant of 80 is assigned to the bulk solvent and a low dielectric constant of 2 to the interior of the protein and membrane. The water inside the channel is assigned a dielectric constant of 60, based on the work of Ng et al.⁴³ Partial charges are placed at the center of each atom, according to the charmm force field. The electric field of the channel is then calculated on a mesh of grid points, using the APBS program,⁴¹ and the results are stored in the lookup table. Forces on ions and partial charges in the blocker molecule are calculated during the simulation by interpolating from this grid. This means that both ions as well as atoms in the blocker molecule are treated as if they had the same high dielectric constant as the bulk solvent. They do not contribute to the dielectric boundary, which is defined solely by the channel and lipid slab. This approximation is known as the test charge approximation. It may cause some close contact descreening effects to be ignored. We instead lump any such effects into a phenomenological low-resolution term that describes hydrogen bonding and salt bridges.

The second category of channel and solvent mediated electrostatic forces are those due to fields originating from the mobile charges themselves. The linearity of Poisson's equation means that the total electric field due to these forces is the sum of the individual fields generated by single charges. Since the mobile charges move around during the simulation, the use of lookup tables becomes more difficult. A lookup table would ideally give the field at every grid point (three dimensions) generated by a charge at another grid point (three dimensions) and would thus have a six-dimensional domain. This is not computationally efficient, and thus we are forced to approximate these effects using a simplified cylindrically symmetric boundary for the channel. Given the cylindrical boundary, the geometry and solution method are described in detail by Hoyles et al.⁴⁴ A three-dimensional cylindrical grid is defined, and the symmetric boundary is then used to calculate the electric field at all grid points induced by an ion located at each grid point. This allows us to store a two-dimensional lookup table describing the interaction of an ion with its own image charge in the dielectric boundary and a five-dimensional lookup table describing the interaction of an ion with the image charge of another ion. A further three-dimensional lookup table is defined by solving Poisson's equation using the same symmetric boundary and applying a constant electric field; this allows us to take into account the effect of the membrane potential, which is not as easily done using APBS.

How best to define the cylindrical boundary used in this approximation is to some extent an open question. One method, which has been used in previous ion permeation studies,¹⁹ is to find the locus of all atoms in the channel as they rotate around the pore axis and smooth the resulting boundary by tracing with a water sphere. While this works well for ion permeation in nearly cylindrical pores, it is not ideal for blocker binding, because the blocker often binds by lodging atoms in crevices in the channel wall, which might be located well inside the cylindrical boundary. Another method, which we have used for small blockers,¹³ is to remove a few surface atoms from the boundary definition, in order to make room for the bound complex. However, this method does not work well for large polypeptide toxins, as too many channel atoms would need to be excised, distorting the electrostatics. Thus, for the current case, we have defined the boundary by effectively forming an angular average over the three-dimensional solvent accessible surface of the pore,

so that the cylindrical radius of the channel for a given z represents an average radius for the channel over all radial angles. Furthermore, we modify our previous system so that the cylindrical radius no longer acts as a physical barrier to mobile atoms. Instead, they may be able to pass a small distance beyond the boundary at certain locations. In such cases, the force is calculated by mapping the radial coordinate back to the surface of the cylindrical boundary, minus a small buffer, and finding the force at that point. The practical upshot is that there is a continuous force present that acts to prevent charges from passing too far inside the boundary, due to the image charge effect.

Nonpolar Hydration Forces. van der Waals interactions between solute atoms and water molecules, as well entropic effects due to the water, can play a large role in biomolecular binding. Most notable is the hydrophobic force. When water contacts a hydrophobic surface, extra water–water hydrogen bonds are formed. The resulting reduction in entropy incurs a free energy penalty, making the situation unfavorable. Such effects mean that the short-range nonpolar forces that exist between solute molecules in the presence of water can be very

$$U(r_{12}) = \begin{cases} U_0 \left(\frac{1}{2} - \frac{3}{2} \left[\frac{r_{12} - R_1 - R_2 - w/2}{w} \right] + 2 \left[\frac{r_{12} - R_1 - R_2 - w/2}{w} \right]^3 \right), & 0 \leq r_{12} - R_1 - R_2 \leq w, \\ 0 & \text{otherwise} \end{cases} \quad (3)$$

For an attractive potential, $U_0 < 0$, the potential attains its most negative value when the atoms are just touching ($r_{12} = R_1 + R_2$) and goes smoothly to zero over a distance w . Our choices for parameters U_0 and w are based on observations made over extensive simulations under different conditions but not on a systematic optimization of the force field. Along with the other parameters in our model, they lead to realistic potentials of mean force for blocker binding. We use $U_0 = -0.017$ kcal/mol for nonhydrophobic residues and $U_0 = -0.034$ kcal/mol for hydrophobic residues, with $w = 3$ Å in both cases.

Salt Bridges and Hydrogen Bonding. The formation of salt-bridges between basic residues on the toxin and acidic residues in the outer vestibule of the channel are important to binding. In the current work, hydrogens are not modeled explicitly, and we therefore add extra terms to the force field to account for these salt bridges. We use a low-resolution potential, with a single force center for each heavy atom involved in the bonding. The force centers are located at the center of the NZ for Lys, NH1 and NH2 for Arg, OD1 and OD2 for Asp, and OE1 and OE2 for Glu. We use the same functional form used to model nonpolar forces, eq 3, with $w = 4$ Å, and $U_0 = 0.43$ kcal/mol when one of the atoms is from a Lys residue and $U_0 = 0.22$ kcal/mol when one of the atoms is from an Arg, so as to put the two force centers of Arg on an equal footing with the one force center of Lys.

Potentials of Mean Force. To derive potentials of mean force (PMFs) for the interaction between the blocker and the channel, umbrella sampling combined with the weighted histogram analysis method (WHAM) is employed. A series of umbrella windows are used, with the center of mass of the blocker being harmonically constrained to a different value of z in each window. The trajectories of the blocker center of mass are then fed into the WHAM program⁴⁵ to compute a one-dimensional PMF. Note that the one-dimensional PMF becomes ill-defined in regions where the blocker is not radially constrained by interaction with the channel; this is due to the fact that one-dimensional PMFs

different from those that exist in the absence of water, i.e., the bare Lennard-Jones interactions. Unfortunately, they have proved to be hard to accurately model. Most implicit solvent models use a potential that is proportional to the solvent accessible surface area, perhaps augmented by a term proportional to the volume. Multipliers are sometimes used for different atom types, e.g., hydrophobic vs hydrophilic.

Brownian dynamics uses rigid bodies (the blockers), fixed bodies (the channel), and single ions. Surface area dependent effects can therefore be efficiently incorporated using a short-range pair potential, since only surface–surface contacts can occur between rigid and fixed bodies, and the contact area can be approximated using these short-range pair potentials. This pair potential can depend on the atom types involved in the interaction, and is designed to represent the combined effect of water-mediated nonpolar interactions between simulation atoms as well as the hydrophobic effect and other nonpolar hydration effects. We employ a short-range switching pair potential of the form in eq 3.

include an entropic contribution that is proportional to the negative logarithm of the area explored by the blocker, so an unconstrained blocker would in theory give an infinitely deep well. For this reason, we also constrain the blocker to a cylinder of radius 2 Å around the average (x, y) coordinate of the bound blocker, which provides a reasonable compromise between allowing the blocker to explore various binding conformations and the simulation time needed in order to achieve convergence.

Model of the NavAb Channel. The crystal structure of the bacterial NavAb voltage gated sodium channel was recently determined,²¹ making it the first sodium channel to have its structure solved. The channel contains a number of interesting features, and presents an exciting opportunity for computational structure-function studies. Like other voltage gated ion channels, the bacterial sodium channel is a homotetramer, with each monomer consisting of six membrane spanning segments, labeled S1 to S6. The pore module is formed by segments S5–S6, which are connected by a P-loop forming a narrower selectivity filter at the exoplasmic side of the pore as well as the outer vestibule of the pore. Surrounding the pore module, segments S1–S4 make up the voltage sensing mechanism. On the intracellular side of the pore, the end of segment S6 forms the intracellular gate of the pore. In the crystal structure published by Payandeh et al.,²¹ the gate is closed, despite the voltage sensors being in their activated conformation, suggesting that the channel is in a pre-open conformation. The crystal structure omits the residues 222 and onward downstream of the gate region of S6, which were poorly ordered in the X-ray density. The closed gate, together with the fact that these residues are omitted, means that there is some uncertainty about the precise conformation of gate region when the channel is open.

An initial channel model is first constructed, based on crystal structure 3RVY from the RCSB Protein Data Bank.²¹ After building a tetramer based on crystallographic information in the PDB file, the gate, which was initially occluded, is opened somewhat during

the refinement step using constrained minimization, with segments S1–S5 being highly constrained to the initial crystal structure using force constants of 50 kcal/mol Å² and 5 kcal/mol Å² for the backbone and side chains respectively, and segment S6, which forms the inner pore, being only weakly constrained using a force constant of 1 kcal/mol Å². To open the gate, we simply apply a repulsive cylindrical potential centered along the pore axis. This procedure is consistent with the speculation by Payandeh et al. that the gate may open by a subtle dilation.²¹ Figure 2 shows the pore profile calculated after refinement and molding.

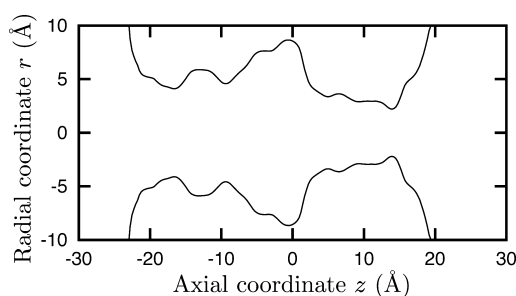


Figure 2. Pore profile for the reshaped channel.

To further prepare the channel model for use in Brownian dynamics, we truncate residues 1–104, resulting in the removal of the voltage sensing domains S1–S4, and giving a neutral pore.

RESULTS AND DISCUSSION

The main purpose of this paper is to demonstrate new techniques for simulating ion channel blockers using Brownian dynamics by applying our program to the NavAb channel and the μ -conotoxin PIIIA blocker. However, before looking at blocker binding, it is important to validate aspects of our channel model by exploring aspects of the energetics and permeation of the pore.

Channel Energetics. To gain insight into the pore energetics, we compute one and two ion potentials of mean force. These PMFs are constructed by direct numerical integration of Boltzmann factors over all coordinates orthogonal to the reaction coordinate. For example, for a single-ion one-dimensional PMF, we integrate over discs perpendicular to the z axis; for a two-ion one-dimensional PMF we also integrate over all positions of the second ion. The blue curve in Figure 3A depicts the one-dimensional potential of mean force experienced by a single sodium ion confined within 3 Å of the channel axis. There is an energy well of around 20 kT in depth, with the deepest point occurring inside the selectivity filter. Note that this is much shallower than the well inside potassium channels,¹⁹ due in large part to the wider selectivity filter in the NavAb channel. The red line depicts the PMF when the channel already contains another ion that is free to move in thermodynamic equilibrium. The well depth has been halved by the presence of the second ion, and a barrier of only around 6–7 kT exists between the filter and the intracellular entrance to the pore. This is consistent with a linear current voltage relationship. In contrast, high barriers separating binding sites would imply a nonlinear curve, and an imbalance between inner and outer binding sites would imply rectification.

In Figure 3B, we see a two-dimensional, two-ion PMF. The horizontal axis represents the z coordinate of the first ion, and the vertical axis the z -coordinate of the second ion. The main conduction pathway is shown as a solid black line. At point 1,

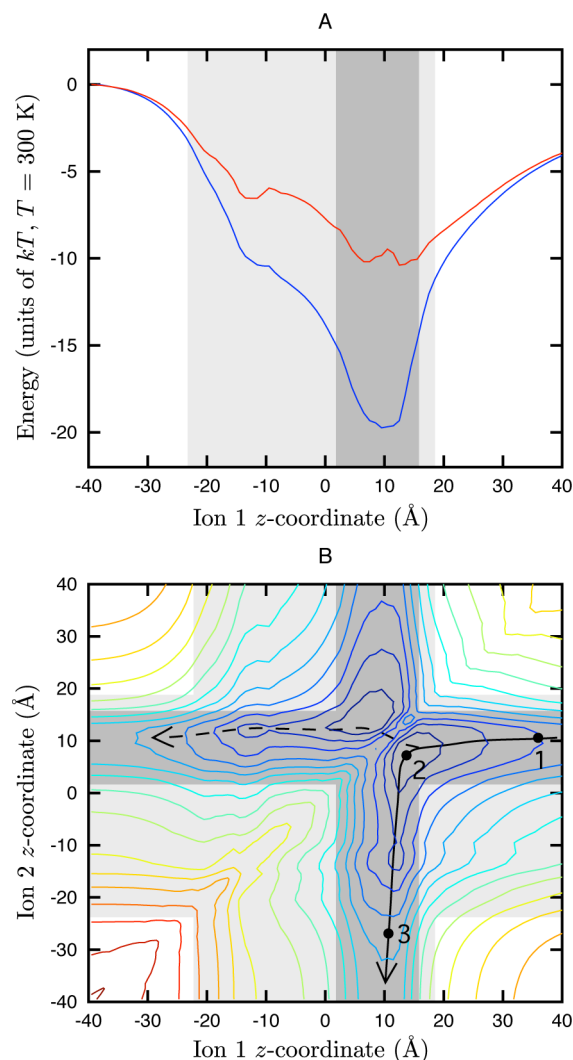


Figure 3. (A) One-dimensional PMF (blue) for an ion confined within 3 Å of the channel axis z . The red curve shows the effect on the PMF of having a second ion already in the channel. Light shading indicates the limits of the pore, and darker shading the limits of the selectivity filter. (B) The two-dimensional energy landscape of the two-ion PMF. Contour lines are spaced at 2 kT intervals. The reaction coordinate is (z_1, z_2) , the z coordinates of ions 1 and 2, respectively. Light and dark shading indicate the limits of the pore and selectivity filter, respectively. The solid path depicts the classic knock-on conduction mechanism, and the dotted path depicts an alternative conduction route, where the two ions move past each other in the filter.

the first ion is in the extracellular space, and the second ion is in the filter at $z \approx 10$ Å. The first ion approaches the pore without having much effect on the position of the second ion until the pore begins to narrow, at around $z = 19$ Å; this can be seen by the fact that the conduction pathway is nearly horizontal. At point 2, both ions are in the filter, and the movement of the first ion pushes the second ion toward the intracellular side. The system has reached its minimum free energy at this point. At point 3, the second ion is about to exit the pore, and the first ion is inside the filter. Thus conduction occurs by a classic two-ion knock-on mechanism. An alternative conduction pathway has the ions moving past each other by overcoming a small energy barrier of around 2 kT. This is shown by the dotted path in the figure. Similar results were obtained using molecular dynamics simulations by Corry and Thomas²⁸ and Furini and Domene,²⁹

although some fine-scale structure seen in the latter two papers is far less prominent in our PMF, most notably, the barrier separating the two binding positions inside the selectivity filter. We interpret this as being due to single water effects in the explicit water molecular dynamics simulations which are not present in our implicit water simulation.

Channel Permeation. The energy landscape seen above suggests a linear current–voltage curve. To investigate the permeation characteristics of the channel, we run Brownian dynamics simulations with a symmetric concentration of 160 mM NaCl. The correct concentration is maintained using the grand canonical Monte Carlo technique.^{32,33} The resulting current–voltage profile is shown in Figure 4. Experimental data from mammalian

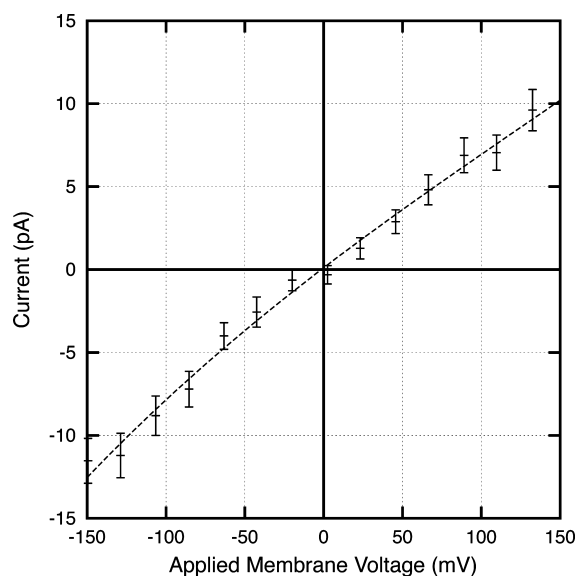


Figure 4. Current voltage profile for the channel.

voltage gated sodium channels²⁶ exhibits an ohmic current–voltage relationship between ± 70 mV, with a conductance of around 20 pS at a symmetric NaCl concentration of 206 mM. More recently, Shaya et al.²⁷ have performed single cell measurements on a pore-portion of the bacterial NavSp1p channel. Using an external concentration of 200 mM NaCl and an internal concentration of 110 mM KCl, they obtained a nearly linear current–voltage curve, whose inward (sodium) current has a conductance of around 50 pS. Despite the fact that none of the experimental data apply to NavAb, our curve is reminiscent of the experimental results, being nearly ohmic over its range and having a conductance of 70 pS over the ± 100 mV range.

We can gain a greater insight into the channel permeation by looking at the dwell histogram for the ions. Figure 5A shows the linear number density of all ions within a 5 Å radius of the channel axis. In Figure 5B, this is converted into a potential of mean force for a single ion in the presence of all other ions in the system. Moving from the extracellular to intracellular side of the channel, we see two binding sites inside the filter. The inner vestibule presents a larger barrier of 3 kT, which is assumed to be the rate limiting step in the conduction process. There is in addition a minor binding site visible some distance inside the intracellular gate, at $z = -12$ Å, which is assumed to be due to the presence of the adjacent negatively charged Asp-219 residues as well as the small widening of the channel at that point. In addition, there is a build up of sodium ions in the

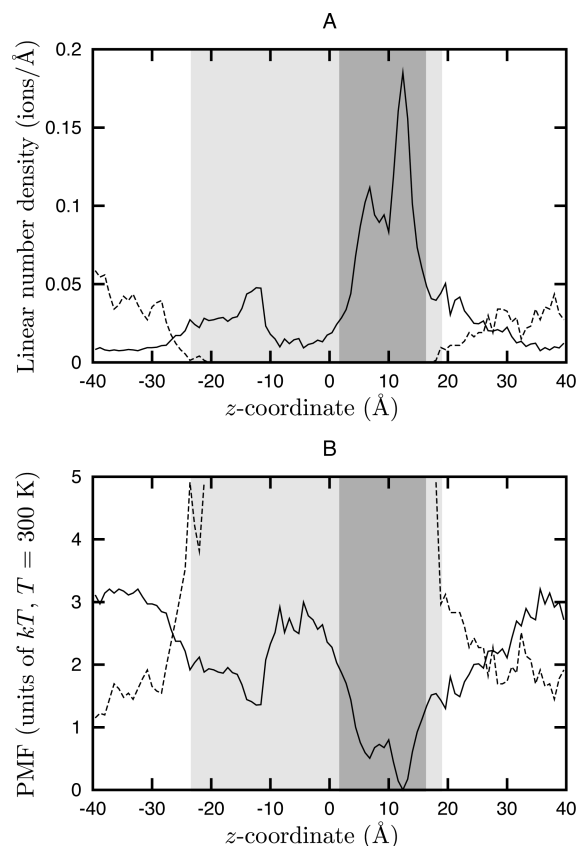


Figure 5. Dwell histogram for the channel. (A) The linear number density of cations (solid line) and anions (dashed line) dwelling within a radius of 5 Å from the channel axis. Merged peaks can be seen at around 6–12 Å, representing ion binding sites inside the filter. Between $z \approx 20$ and 30 Å, a rise in the concentration of cations in the outer vestibule of the channel is apparent, due to negative changes in the protein. (B) The negative logarithm of the density, which can be interpreted as a potential of mean force for a single ion in the presence of all other ions in the system.

negatively charged external vestibule of the channel, at around $z = 20$ –30 Å.

The conduction process itself is shown in Figure 6. Conduction occurs in most instances by a knock-on mechanism, with one or two ions dwelling in the filter. An ion approaches from the outer vestibule and enters the pore, destabilizing the innermost ion and causing it to move into the inner cavity and from there into the intracellular medium. The red band seen at around 20–30 Å represents a concentration of sodium ions, due to negative charges in the outer vestibule.

Spontaneous Binding of Blockers to the Channel (Docking). Using our rigid-body Brownian dynamics simulation, we recreate a possible block mechanism of the channel by the μ -conotoxin PIIIA (cone snail) toxin. Based on a previous molecular dynamics study by Chen and Chung,¹⁴ we begin with two already docked toxin–channel complexes, shown in Figure 7. The first, complex A, has the blocker Arg-2 inserted into the pore, and the second, complex B, has the blocker Lys-9 inserted into the pore. The reader should keep in mind that these two complexes exhibit conformational differences in the outer vestibule of the channel. In complex A, two Met-181 residues in the channel move inward to contact with hydrophobic residues in the blocker. These residues partly obscure the entrance to the pore, potentially complicating the application of rigid body

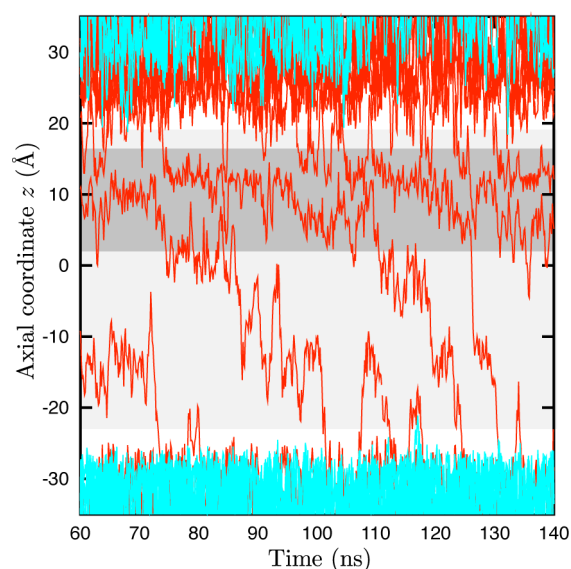


Figure 6. Typical segment of the permeation trajectory. The horizontal axis represents time, and the vertical axis the z coordinate, along the axis of the channel. Red lines represent the trajectories of sodium ions, and blue the trajectories of chloride ions. The membrane voltage was set to approximately -60 mV. The pore is indicated by light gray shading, and the filter by darker gray.

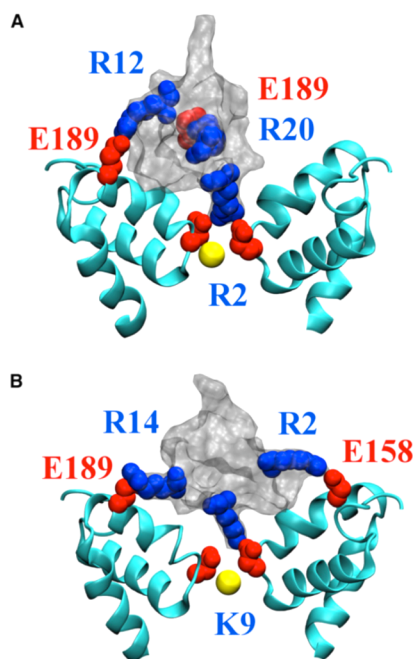


Figure 7. Binding modes of the toxin that is used to obtain the rigid models of the blocker. (A) The toxin docks with Arg-2 inserted into the pore. (B) The toxin docks with Lys-9 inserted into the pore. Figure reproduced from Chen and Chung.¹⁴

Brownian dynamics. In complex B, there is some general widening of the outer vestibule, but the entrance to the pore remains largely the same as the original channel model.

In view of the fact that we do not currently incorporate flexibility into our Brownian dynamics simulation, we use the channel and blocker conformations from both of these complexes as a starting point for our simulations. We perform an initial constrained energy minimization to build hybrid models of the initial Brownian dynamics model used for the permeation

study and the docked complex A or B. Atoms in the channel are all strongly constrained, with the outer vestibule atoms that lie near the blocker being constrained to the docked coordinates, and the rest of the channel being constrained to our initial model. The charged side chains of the blocker are weakly constrained to their docked positions, and the other blocker atoms are strongly constrained to the docked positions. This procedure gives us three channel models to work with: channel model A whose outer vestibule is configured to accept the blocker with Arg-2 inserted into the pore, channel model B, whose outer vestibule is configured to accept the blocker with Lys-9 inserted into the pore, and the original channel model used for the permeation results. Similarly, we have two blocker models, A and B.

For our investigation of spontaneous docking, we perform four sets of simulations: channel model A with blocker model A, channel model B with blocker model B, the original channel model with blocker model A, and the original channel model with blocker model B. Twenty independent runs of 100 ns each are performed in each case. The blocker is initially placed in the extracellular medium some 20 Å from its docked position, and with a random orientation for each of the twenty runs, and is free of any constraints during the simulation.

A typical binding event is shown in Figure 8. The positively charged blocker is initially drawn to the negatively charged extracellular vestibule of the channel (A). It tumbles for a time in the vestibule (B), making and breaking salt bridges and hydrophobic contacts, until the bound state is achieved (C). The bound configuration then persists quasi-permanently.

We find that the blocker is bound to the channel during 38–59% of the total runtime in three out of the four cases studied. These three cases are typified by Figure 9, in which the original channel, not modified to conform to the blocker, is used. A variety of binding modes, including the two modes A (Arg-2 in pore) and B (Lys-9 in pore) studied in this paper, are seen. This is consistent with the multiple binding modes identified in Chen and Chung.¹⁴ The fact that even the unmodified channel can be used to achieve successful docking is encouraging. Of the four cases studied, only the case of channel model A, with the pore modified to conform to the bound state where Arg-2 inserts into the pore, exhibits a low degree of binding, some 3% of the total runtime. We interpret this as being due to the pore being partially obstructed by two methionine residues in this case, as discussed previously, meaning that very precise maneuvers are needed for the blocker to enter the pore.

Potentials of Mean Force for the Bound Blocker. We obtain the potential of mean force (PMF) for the channel-toxin binding process, as explained in the Theory and Methods section. Figure 10 shows the PMFs for channel/blocker models A and B. 100 ns of data was used for each umbrella window. The PMF is some 22 kT in depth for model A (i.e., Arg-2 in the pore) and 25 kT for model B (i.e., Lys-9 in the pore). Beyond a distance of around 30 Å, the blocker is attracted to the mouth of a pore by a broad electrostatic potential well. Closer than this distance, the well slopes rapidly downward due to the effects of hydrophobic and salt bridges coming into play as well as the increased electrostatic attraction of the pore.

Given the PMF, we can calculate the dissociation constant for the blocker–channel interaction using the usual formula.^{12,13,46}

$$K_d^{-1} = 1000\pi R^2 N_A \int_{z_1}^{z_2} \exp(-W(z)/kT) dz \quad (4)$$

where z_1 and z_2 give the limits of the binding site, $W(z)$ is the one-dimensional PMF, with the zero-point of energy set to be zero in

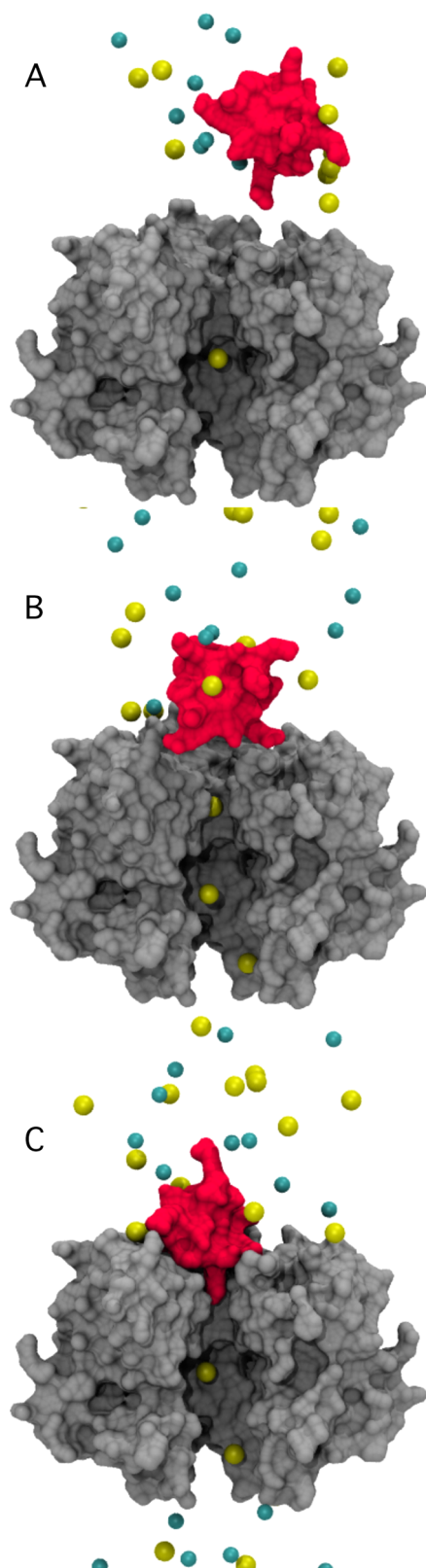


Figure 8. Typical binding sequence, involving the bound state where Lys-9 is inserted into the pore. The total time for the sequence is 50 ns. (A) The blocker approaches from the extracellular medium, (B) tumbles in the extracellular vestibule of the channel, and (C) binds strongly to the channel, with Lys-9 inserted into the pore.

the bulk, N_A is Avogadro's number, k is Boltzmann's constant, and T is the temperature. The factor of $1000N_A$ is a conversion from m^3

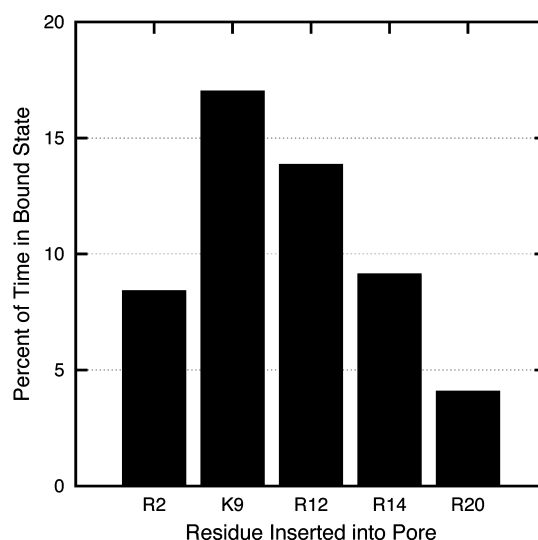


Figure 9. Percentage of time spent in various bound states. The bound states are labeled by the residue number of the residue that inserts into the pore. Values are averaged for 20 independent runs of 100 ns each. Results were obtained using the unmodified channel model.

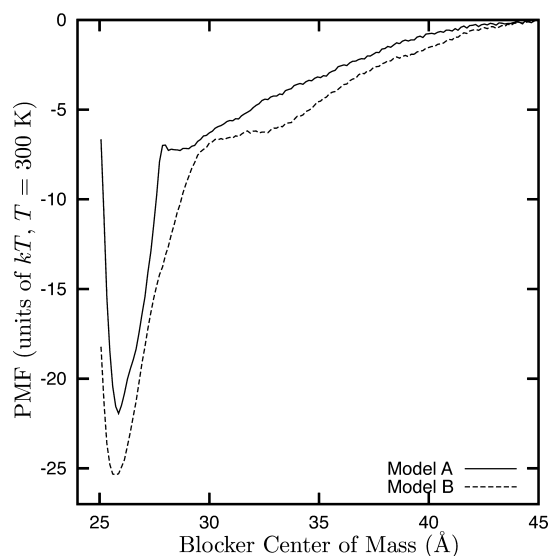


Figure 10. Potentials of mean force for the toxin unbinding from the channel.

(per atom) to L/mol. For the data presented here, we derive a dissociation constant of 95 nM for model A and 1.9 nM for model B.

These values are similar or lower than experimentally determined values for mammalian channels.^{30,31} Data are not available for the bacterial channel. In molecular dynamics simulations, Chen and Chung derived binding constants of the order of 0.1 nM or less and nearly identical binding affinities for each of the two bound states studied here. Given that we have yet to include any flexibility in our model and the general uncertainties inherent in experimental results, the agreement is reasonable, and at this stage, our model should be treated as a plausible model of blocker binding that would require further verification to be sure if it is correct in its details.

CONCLUSIONS

This work presents significant advances in our Brownian dynamics simulations of interactions between ion channels,

ions and channel blocker molecules. Carrying on from previous work¹³ which simulated the interaction between a small charged molecule and an ion channel, we investigate the ability of Brownian dynamics to simulate interactions involving larger polypeptide toxins. We carry out our simulations on the bacterial NavAb channel, whose crystal structure was only recently elucidated. By opening the intracellular gate of the crystal structure channel, we compute a current–voltage relationship that is consistent with experimental studies on mammalian NaV channels.^{26,27} Moving on to investigate the binding of μ -conotoxin P11A to the channel, we perform rigid-body Brownian dynamics simulations on docked conformations of the channel and blocker that appear able to capture much of the energetics and dynamics of channel-blocker interactions. We derive potentials of mean force for toxin unbinding that, despite experimental and computational uncertainties, are in general agreement with experimental binding energies^{30,31} and molecular dynamics calculations.¹⁴ Our simulations cover many microseconds, with the potential to cover a good deal more where necessary.

At present, our model exhibits some limitations. Further development would lead to a tool that would be extremely useful for the purpose of drug discovery and development. First, in this paper we have performed calculations using predocked conformations of the channel and blocker; in the future we will need to introduce some flexibility into the model. Using flexible (hinged) side chains of important residues would be an easy and computationally efficient way to handle this. Second, we have used some simple methods to handle the close-range electrostatic and nonpolar interactions between the blocker and channel molecules. The parameters used in these methods have been adjusted by hand to help to obtain realistic results. In the future, we would like to perform some kind of more systematic fitting of parameters that is tailored specifically to interactions between polypeptide toxins and the outer vestibules of various ion channels. By doing so, we would hope to derive models that can be usefully used to make accurate predictions that are tailored to this limited domain. This work would be carried out using a larger sample set consisting of several different channels and blockers and would demonstrate the more general application of our techniques. Further developments of the methodology for representing nonpolar and near field electrostatic interactions are also being investigated. Although we have not yet achieved our ultimate aims, we have made significant progress and are confident that success would add another extremely useful tool in a field that is clearly in need of further progress.

AUTHOR INFORMATION

Corresponding Author

*E-mail: dan.gordon@anu.edu.au.

Notes

The authors declare no competing financial interest.

ACKNOWLEDGMENTS

The calculations upon which this work is based were carried out using a SGI Altix 3700 system of the Australian National University Supercomputer Facility. This work is supported by grants from the NHMRC. We thank Rong Chen for providing Figure 7.

REFERENCES

- (1) Ashcroft, F. *Ion channels and Disease: Channelopathies*; Academic Press: San Diego, CA, 2000.
- (2) Fernández-Ballester, G.; Fernández-Carvajal, A.; González-Ros, J. M.; Ferrer-Montiel, A. *Pharmaceutics* **2011**, *3*, 932–953.
- (3) Wulff, H.; Castle, N. A.; Pardo, L. A. *Nat. Rev. Drug Discov.* **2009**, *8*, 982–1001.
- (4) Hille, B. *Ion Channels of Excitable Membranes*; Sinauer: Sunderland, MA, 2001.
- (5) Kew, J.; Davies, C. *Ion Channels: from Structure to Function*; Oxford University Press: Oxford, U.K., 2010.
- (6) Bogin, O. *Modulator* **2006**, *21*, 28–31.
- (7) Jensen, M. Ö.; Borhani, D. W.; Lindorff-Larsen, K.; Maragakis, P.; Jogini, V.; Eastwood, M. P.; Dror, R. O.; Shaw, D. E. *Proc. Natl. Acad. Sci. U.S.A.* **2010**, *107*, 5833–5838.
- (8) Woo, H.-J. *Methods Mol. Biol.* **2008**, *443*, 109–120.
- (9) Baştuğ, T.; Chen, P.; Patra, S.; Kuyucak, S. *J. Chem. Phys.* **2008**, *128*, 155104–1–155104–9.
- (10) Chen, P. C.; Kuyucak, S. *Biophys. J.* **2009**, *96*, 2577–2588.
- (11) Chen, P. C.; Kuyucak, S. *Biophys. J.* **2011**, *100*, 2466–2474.
- (12) Chen, R.; Robinson, A.; Gordon, D.; Chung, S. H. *Biophys. J.* **2011**, *101*, 2652–2660.
- (13) Gordon, D.; Chen, R.; Ho, J.; Coote, M. L.; Chung, S.-H. *J. Phys. Chem. B* **2012**, *116*, 1933–1941.
- (14) Chen, R.; Chung, S. H. *Biophys. J.* **2012**, *102*, 483–488.
- (15) Chen, R.; Chung, S. H. *Biochemistry* **2012**, *51*, 1976–1982.
- (16) Meng, X.-Y.; Xu, Y.; Zhang, H.-X.; Mezei, M.; Cui, M. *J. Biomed. Biotechnol.* **2012**, *2012*, 121034–1–121034–11.
- (17) Cornell, W.; Cieplak, P.; Bayly, C.; Gould, I.; Merz, K.; Ferguson, D.; Spellmeyer, D.; Fox, T.; Caldwell, J.; Kollman, P. *J. Am. Chem. Soc.* **1995**, *117*, 5179–5197.
- (18) Srinivasan, J.; Cheatham, T., III; Cieplak, P.; Kollman, P.; David, A. *J. Am. Chem. Soc.* **1998**, *120*, 9401–9409.
- (19) Chung, S. H.; Allen, T. W.; Kuyucak, S. *Biophys. J.* **2002**, *82*, 628–645.
- (20) Gordon, D.; Chung, S. H. *Biophys. J.* **2011**, *101*, 2671–2678.
- (21) Payandeh, J.; Scheuer, T.; Zheng, N.; Catterall, W. A. *Nature* **2011**, *475*, 353–358.
- (22) Shon, K. J.; Olivera, B. M.; Watkins, M.; Jacobsen, R. B.; Gray, W. R.; Floresca, C. Z.; Cruz, L. J.; Hillyard, D. R.; Brink, A.; Terlau, H.; Yoshikami, D. *J. Neurosci.* **1998**, *18*, 4473–4481.
- (23) Nielsen, K. J.; Watson, M.; Adams, D. J.; Hammarström, A. K.; Gage, P. W.; Hill, J. M.; Craik, D. J.; Thomas, L.; Adams, D.; Alewood, P. F.; Lewis, R. J. *J. Biol. Chem.* **2002**, *277*, 27247–27255.
- (24) McArthur, J. R.; Ostroumov, V.; Al-Sabi, A.; McMaster, D.; French, R. J. *Biochemistry* **2010**, *49*, 116–124.
- (25) McArthur, J. R.; Singh, G.; O'Mara, M. L.; McMaster, D.; Ostroumov, V.; Tieleman, D. P.; French, R. J. *Mol. Pharmacol.* **2011**, *80*, 219–227.
- (26) Schild, L.; Moczydlowski, E. *Biophys. J.* **1994**, *66*, 654–666.
- (27) Shaya, D.; Kreir, M.; Robbins, R. A.; Wong, S.; Hammon, J.; Brüggemann, A.; Minor, D. L., Jr. *Proc. Natl. Acad. Sci. U.S.A.* **2011**, *108*, 12313–12318.
- (28) Corry, B.; Thomas, M. *J. Am. Chem. Soc.* **2012**, *134*, 1840–1846.
- (29) Furini, S.; Domene, C. *PLoS Comp. Biol.* **2012**, *8*, e1002476–1–e1002476–7.
- (30) Safo, P.; Rosenbaum, T.; Shcherbatko, A.; Choi, D.; Han, E.; Toledo-Aral, J.; Olivera, B.; Brehm, P.; Mandel, G. *J. Neurosci.* **2000**, *20*, 76–80.
- (31) Wilson, M.; Yoshikami, D.; Azam, L.; Gajewiak, J.; Olivera, B.; Bulaj, G.; Zhang, M. *Proc. Natl. Acad. Sci. U.S.A.* **2011**, *108*, 10302–10307.
- (32) Im, W.; Seefeld, S.; Roux, B. *Biophys. J.* **2000**, *79*, 788–801.
- (33) Corry, B.; Hoyle, M.; Allen, T. W.; Walker, M.; Kuyucak, S.; Chung, S. H. *Biophys. J.* **2002**, *82*, 1975–1984.
- (34) Kubo, R. *Rep. Prog. Phys.* **1966**, *29*, 255–284.
- (35) van Gunsteren, W. F.; Berendsen, H. J. C. *Mol. Phys.* **1982**, *45*, 637–647.
- (36) Gordon, D.; Hoyle, M.; Chung, S. H. *Phys. Rev. E* **2009**, *80*, 066703–1–066703–12.
- (37) de la Torre, J. G.; Huertas, M. L.; Carrasco, B. *Biophys. J.* **2000**, *78*, 719–730.

- (38) Weeks, J. D.; Chandler, D.; Andersen, H. C. *J. Chem. Phys.* **1971**, *54*, 5237–5247.
- (39) Tan, C.; Tan, Y.-H.; Luo, R. *J. Phys. Chem. B* **2007**, *111*, 12263–12274.
- (40) Corry, B.; Allen, T. W.; Kuyucak, S.; Chung, S. H. *Biophys. J.* **2001**, *80*, 195–214.
- (41) Baker, N. A.; Sept, D.; Joseph, S.; Holst, M. J.; McCammon, J. A. *Proc. Natl. Acad. Sci. U.S.A.* **2001**, *98*, 10037–10041.
- (42) Nina, M.; Im, W.; Roux, B. *Biophys. Chem.* **1999**, *78*, 89–96.
- (43) Ng, J. A.; Vora, T.; Krishnamurthy, V.; Chung, S. H. *European Biophys. J.* **2008**, *37*, 213–222.
- (44) Hoyles, M.; Kuyucak, S.; Chung, S. H. *Comput. Phys. Commun.* **1998**, *115*, 45–68.
- (45) Grossfield, A. *Weighted Histogram Analysis Method*. <http://membrane.urmc.rochester.edu/wham/index.html>.
- (46) Allen, T.; Andersen, O. S.; Roux, B. *Proc. Natl. Acad. Sci. U.S.A.* **2004**, *101*, 117–122.